DOI: 10.19884/j.1672-5220.202407005

Static Characteristic Analysis of Aerostatic Porous Bearing with a Restricted Layer

YU Zhe[1,2], YAN Ruzhong[1,2*], MA Xiaojian[1,2], ZHANG Haojie[1,2]
1. College of Mechanical Engineering, Donghua University, Shanghai 201620, China
2. Engineering Research Center of Advanced Textile Machinery, Ministry of Education, Donghua University, Shanghai 201620, China

Abstract: To enhance the gas-damping effect and improve the bearing performance, a restricted layer is applied on the surface of aerostatic porous bearings. Based on the gas lubrication theory, a mathematical model of an aerostatic porous bearing with a restricted layer is established, and two proportional coefficients, a permeability ratio δ and a thickness ratio γ, are proposed. Critical values of δ and γ are determined through sensitivity analyses of complex restriction-layer parameters. The static characteristics of aerostatic porous bearings with a restricted layer or an unrestricted layer are comparatively analyzed by using Fluent simulation. The results show that when $\delta \approx 0.005$ and $\gamma \approx 0.010$, the load capacity and static stiffness of the restricted-layer aerostatic porous bearing are high; compared with the unrestricted-layer aerostatic porous bearing, the restricted-layer aerostatic porous bearing has a lower sensitivity to changes in the air supply area. The existence of the restricted layer not only enhances the throttling effect and reduces the mass flow rate, but also effectively improves the static stiffness of the bearing.

Keywords: aerostatic porous bearing; restricted layer; static characteristic; critical coefficient
CLC number: TH133.36 **Document code**: A
Article ID: 1672-5220(2025)05-0543-07

Open Science Identity (OSID)

0 Introduction

The porous material in aerostatic porous bearings has a uniform structure, and its throttle holes are made up of thousands of tiny air holes with uniform internal fluid movement. Compared with traditional hydrostatic aerostatic bearings, the aerostatic porous bearing has a higher static stiffness and load capacity, and it is the key component of rotary spindles and moving guides for precision machine tools[1-3].

Many researchers have studied the static characteristics of aerostatic porous bearings. Wang et al.[4] investigated the relationship between the air supply pressure, material thickness, elastic modulus and the deformation of the porous bearing, and found that the deformation was directly proportional to the air supply pressure and inversely proportional to the material thickness and elastic modulus. Yan et al.[5] analyzed the static and dynamic characteristics of the vacuum preloaded porous aerostatic bearing. San Andrés et al.[6] built a test rig for the porous tilting pad bearing and tested the effects of the pressure and rotational speed on the static and dynamic characteristics of the bearing. Kang et al.[7] used Fluent simulation to analyze the temperature and pressure distributions of the flow field of the porous mass radial bearing, and the results showed that the maximum temperature occurred at the gas film outlet.

However, due to the compressibility of air, aerostatic porous bearings are prone to pneumatic hammer instability, which causes problems such as increased vibration and noise, shortened bearing life, and impact on bearing stability and accuracy[8-10]. A restricted layer is usually coated on the surface of the aerostatic porous bearing to improve the gas-damping effect and bearing stability and stiffness. Miyatake et al.[11] proposed a bearing with a restricted layer being coated on aerostatic porous material and proved that it could improve the stability of the bearing. Cui et al.[12] proposed that the flow of fluid over the aerostatic porous material and surface restriction layer obeyed Darcy's law and experimentally verified the theoretical model. Saha et al.[13] theoretically analyzed the static characteristics of two-layer (coarse layer) aerostatic porous bearings. The presence of the restricted layer reduced the friction and mass flow in the bearing. Yoshimoto et al.[14] discussed the effect of the restricted layer on the static characteristics of the aerostatic porous bearing under symmetric and coupled loads, respectively, and introduced the surface confinement ratio associated with the restricted layer. Feng et al.[15] analyzed the temperature field of the restricted-layer aerostatic porous bearing. Under high speed and heavy load conditions, the high-temperature heat generated by the air film would be transferred to the rotating spindle, and the thermal expansion and thermal deformation would have a significant effect on the performance of the bearing.

Received date: 2024-07-20
* Correspondence should be addressed to YAN Ruzhong, email: yanrz@dhu.edu.cn
Citation: YU Z, YAN R Z, MA X J, et al. Static characteristic analysis of aerostatic porous bearing with a restricted layer[J]. *Journal of Donghua University (English Edition)*, 2025, 42(5): 543-549.

Although some results have been achieved in the study of the aerostatic porous bearing with a restricted layer, they mainly focus on the influence of restricted-layer coefficients on the static characteristics of the bearing, and there is a lack of comparative analyses of the static characteristics of aerostatic porous bearings with a restricted layer or an unrestricted layer, unable to reflect the superiority of the structure and performance of the restricted-layer aerostatic porous bearing. Therefore, based on the gas lubrication theory, this paper establishes a mathematical model of the restricted-layer aerostatic porous bearing and proposes two proportional coefficients, a permeability ratio δ and a thickness ratio γ, to study the influence of complex restricted-layer parameters on the static characteristics of the aerostatic porous bearing. Through the sensitivity analyses, two critical values of δ and γ are obtained, and the influence of the restricted layer on the static characteristics of the aerostatic porous bearing is obtained by using Fluent simulation. The static characteristics of the restricted-layer aerostatic porous bearing and the unrestricted-layer aerostatic porous bearing are compared and analyzed to verify the superiority of the restricted-layer aerostatic porous bearing in terms of the structure and its static characteristics.

1 Mathematical Model

The schematic diagram of the restricted-layer aerostatic porous bearing is shown in Fig. 1. Pressurized gas is fed into the porous material through the upper surface of the coarse-layer porous material. The thin restricted-layer porous material has a lower permeability than that of the coarse-layer porous material. In the theoretical analysis, it is assumed that the gas flows in both the coarse layer and the restricted layer of the porous material obey Darcy's law[16].

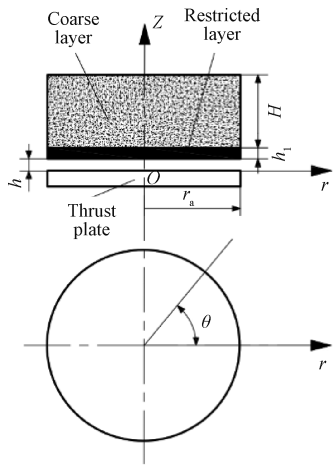

h—bearing clearance; H—thickness of coarse layer; h_1—thickness of restricted layer; r_a—radius of bearing.

Fig. 1 Schematic diagram of restricted-layer aerostatic porous bearing

The analysis is carried out under some assumptions for simplicity.

1) The gas flow is under the isothermal and laminar flow condition and the inertia effect is negligible in the bearing clearance.

2) The cross-film pressure gradient is negligible on the account of the extremely thin gas film.

3) The porous material is deemed to be isotropic, that is, the permeability of the porous material in all directions is equivalent.

Based on the above-mentioned assumptions, the mass flow rates of gases in three directions are

$$m_\theta = -\rho \frac{\varphi}{\mu} \frac{\partial p}{r\partial\theta} \mathrm{d}r\mathrm{d}z, \tag{1}$$

$$m_r = -\rho \frac{\varphi}{\mu} \frac{\partial p}{\partial r} r\mathrm{d}\theta\mathrm{d}z, \tag{2}$$

$$m_z = -\rho \frac{\varphi}{\mu} \frac{\partial p}{\partial z} r\mathrm{d}r\mathrm{d}\theta, \tag{3}$$

where m_θ, m_r and m_z are the mass flow rates of gases in the θ, r and z directions; ρ is the gas density in the external atmosphere; φ is the permeability of the coarse-layer porous material; p is the gas pressure in the bearing clearance; μ is the dynamic viscosity of the gas.

In the numerical calculations, the mathematical model is discretized in three directions (i, j and k), as shown in Fig. 2, and the governing equation of pressure distribution is derived from the continuity of the mass flow in a small element.

According to the law of conservation of masses,

$$m_{\theta\mathrm{in}} - m_{\theta\mathrm{out}} + m_{r\mathrm{in}} - m_{r\mathrm{out}} + m_{z\mathrm{in}} - m_{z\mathrm{out}} = 0, \tag{4}$$

where the subscripts in and out represent the inflow and outflow of gases into and out of the coarse-layer porous material.

Substituting Eqs. (1)–(3) into Eq. (4), we can get the pressure distribution in the coarse-layer porous material:

$$\begin{aligned} &-\rho_\mathrm{b} \frac{\varphi}{\mu} \frac{\partial p_\mathrm{b}}{r\partial\theta}\Big|_{\mathrm{in}} \mathrm{d}r\mathrm{d}z + \rho_\mathrm{b} \frac{\varphi}{\mu} \frac{\partial p_\mathrm{b}}{r\partial\theta}\Big|_{\mathrm{out}} \mathrm{d}r\mathrm{d}z - \\ &\rho_\mathrm{b} \frac{\varphi}{\mu} \frac{\partial p_\mathrm{b}}{\partial r}\Big|_{\mathrm{in}} \left(r + \frac{\mathrm{d}r}{2}\right) \mathrm{d}\theta\mathrm{d}z + \rho_\mathrm{b} \frac{\varphi}{\mu} \frac{\partial p_\mathrm{b}}{\partial r}\Big|_{\mathrm{out}} \left(r - \frac{\mathrm{d}r}{2}\right) \mathrm{d}\theta\mathrm{d}z - \\ &\rho_\mathrm{b} \frac{\varphi}{\mu} \frac{\partial p_\mathrm{b}}{\partial z}\Big|_{\mathrm{in}} r\mathrm{d}r\mathrm{d}\theta + \rho_\mathrm{b} \frac{\varphi}{\mu} \frac{\partial p_\mathrm{b}}{\partial z}\Big|_{\mathrm{out}} r\mathrm{d}r\mathrm{d}\theta = 0, \end{aligned} \tag{5}$$

where the subscript b represents the coarse-layer porous material.

Considering the compressibility of an ideal gas $p_\mathrm{b}/\rho_\mathrm{b} = gRT$, where R is the universal gas constant and T is the gas thermodynamic temperature, Eq. (5) can be transformed as

$$\begin{aligned} &-p_\mathrm{b} \frac{\varphi}{\mu} \frac{\partial p_\mathrm{b}}{r\partial\theta}\Big|_{\mathrm{in}} \mathrm{d}r\mathrm{d}z + p_\mathrm{b} \frac{\varphi}{\mu} \frac{\partial p_\mathrm{b}}{r\partial\theta}\Big|_{\mathrm{out}} \mathrm{d}r\mathrm{d}z - \\ &p_\mathrm{b} \frac{\varphi}{\mu} \frac{\partial p_\mathrm{b}}{\partial r}\Big|_{\mathrm{in}} \left(r + \frac{\mathrm{d}r}{2}\right) \mathrm{d}\theta\mathrm{d}z + p_\mathrm{b} \frac{\varphi}{\mu} \frac{\partial p_\mathrm{b}}{\partial r}\Big|_{\mathrm{out}} \left(r - \frac{\mathrm{d}r}{2}\right) \mathrm{d}\theta\mathrm{d}z - \\ &p_\mathrm{b} \frac{\varphi}{\mu} \frac{\partial p_\mathrm{b}}{\partial z}\Big|_{\mathrm{in}} r\mathrm{d}r\mathrm{d}\theta + p_\mathrm{b} \frac{\varphi}{\mu} \frac{\partial p_\mathrm{b}}{\partial z}\Big|_{\mathrm{out}} r\mathrm{d}r\mathrm{d}\theta = 0. \end{aligned} \tag{6}$$

Introducing the boundary conditions:

$$p_b = p_s \text{ at } z = h + H,$$
$$p_b = p_t \text{ at } z = h + \gamma H,$$
$$\partial p_b / \partial r = 0 \text{ at } r = r_a,$$

where γ is the thickness ratio; p_s is the gas supply pressure; the subscript t represents the restricted layer of the porous material.

Due to the circumferential sealing of the coarse layer, the integrating gives the pressure expression in the coarse layer.

Figure 2 (b) shows the boundary between the restricted-layer and the coarse-layer porous material. The axial gas flow in the restricted layer can be ignored for simplicity considering the negligible thickness, and then the mass flow in the θ and r directions are expressed as

$$m_{\theta t} = -\rho \frac{h^3}{12\mu} \frac{\partial p}{r\partial \theta} \mathrm{d}r, \tag{7}$$

$$m_{rt} = -\rho \frac{h^3}{12\mu} \frac{\partial p}{\partial r} r\mathrm{d}\theta. \tag{8}$$

Similarly, the corresponding pressure distribution equation can be obtained:

$$-p_t \frac{\partial p_t}{r\partial \theta}\Big|_{in} \mathrm{d}r\mathrm{d}z + p_t \frac{\partial p_t}{r\partial \theta}\Big|_{out} \mathrm{d}r\mathrm{d}z -$$
$$p_t \frac{\partial p_t}{\partial r}\Big|_{in} \left(r + \frac{\mathrm{d}r}{2}\right) \mathrm{d}\theta\mathrm{d}z - p_t \frac{\partial p_t}{\partial r}\Big|_{out} \left(r - \frac{\mathrm{d}r}{2}\right) \mathrm{d}\theta\mathrm{d}z -$$
$$2p_t \frac{\partial p_t}{\partial z}\Big|_{in} r\mathrm{d}\theta\mathrm{d}r + 2\delta p_t \frac{\partial p_t}{\partial z}\Big|_{out} r\mathrm{d}\theta\mathrm{d}r = 0, \tag{9}$$

where δ represents the permeability ratio.

Introducing the boundary conditions:

$$p_t = p \text{ at } z = h,$$
$$\partial p_t / \partial r = 0 \text{ at } r = r_a.$$

The junction of the restricted layer and the gas film is shown in Fig. 2 (c). The pressure in the bearing clearance can be expressed as

$$-p \frac{\partial p}{r\partial \theta}\Big|_{in} h^3 \mathrm{d}r + p \frac{\partial p}{r\partial \theta}\Big|_{out} h^3 \mathrm{d}r -$$
$$p \frac{\partial p}{\partial r}\Big|_{in} \left(r + \frac{\mathrm{d}r}{2}\right) h^3 \mathrm{d}\theta + p \frac{\partial p}{\partial r}\Big|_{out} \left(r - \frac{\mathrm{d}r}{2}\right) h^3 \mathrm{d}\theta -$$
$$12\delta\varphi p \frac{\partial p}{\partial z}\Big|_{in} r\mathrm{d}\theta\mathrm{d}r = 0. \tag{10}$$

The load capacity is obtained by substituting the boundary conditions:

$$p = p_a \text{ at } r = r_a,$$

where p_a is the pressure of the external atmosphere.

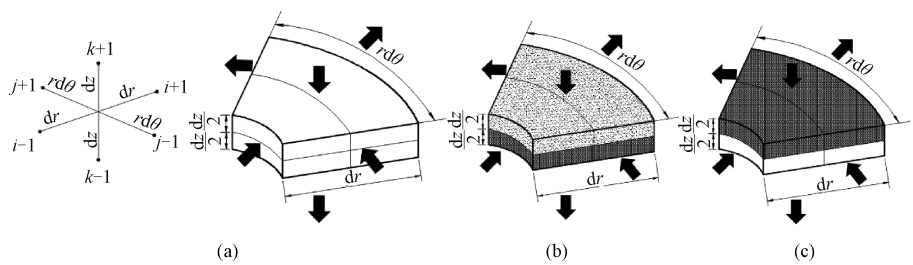

(a) (b) (c)

Fig. 2 Element structures and continuity of mass flow rates: (a) discrete element of porous material; (b) small element in boundary between coarse layer and restricted layer; (c) small element in boundary between restricted layer and bearing clearance

After integrating the pressure distribution over the bearing thrust surface, the bearing stiffness is defined as the rate of change of the load with clearance.

The conventional approach for acquiring performance parameters typically requires solving a set of complex differential governing equations, a process that often entails substantial computational overhead and significant time costs. With the rise and development of finite element software, these troubles could be circumvented by applying a computational fluid dynamics (CFD) approach[17].

2 Numerical Simulation based on Fluent

2.1 Parameters of restricted-layer aerostatic porous bearing

For the restricted-layer aerostatic porous bearing, the permeability and thickness of the restricted layer are principle parameters, and are listed in Table 1. In this paper, the correlation between the parameters of the coarse layer and the restricted layer is taken into account innovatively, introducing the permeability ratio δ and the thickness ratio γ of the restricted layer:

$$\begin{cases} \gamma = \dfrac{h_1}{H}, \\ \delta = \dfrac{\varphi'}{\varphi}, \end{cases} \tag{11}$$

where φ' is the permeability of surface-restricted layer.

Table 1 Principal parameters of restricted-layer aerostatic porous bearing

Parameter	r_a/mm	H/mm	φ/m^2	δ	γ	p_a/MPa	T/K	p_s/MPa	h/μm
Value	15	5	10^{-12}	Variate	Variate	0.1	293	0.5	Variate

2.2 Sensitivity analysis of restricted-layer coefficients

At an air film thickness of 10 μm, the relationship among coefficients (δ and γ) and the bearing performance is obtained. As seen in Fig. 3, as δ increases, the load capacity and the mass flow rate of the bearing increase first and then flatten out at the demarcation value of 0.005, while the static stiffness consistently declines. Furthermore, the higher γ is, the lower the load capacity and the mass flow are, and the slightly higher the static stiffness is. The multi-objective optimization based on CFD made a compromise with bearing performance. It recommends a set of candidate data, namely $\delta \approx 0.005$ and $\gamma \approx 0.010$, where the relatively high load capacity and static stiffness of the bearing can be obtained.

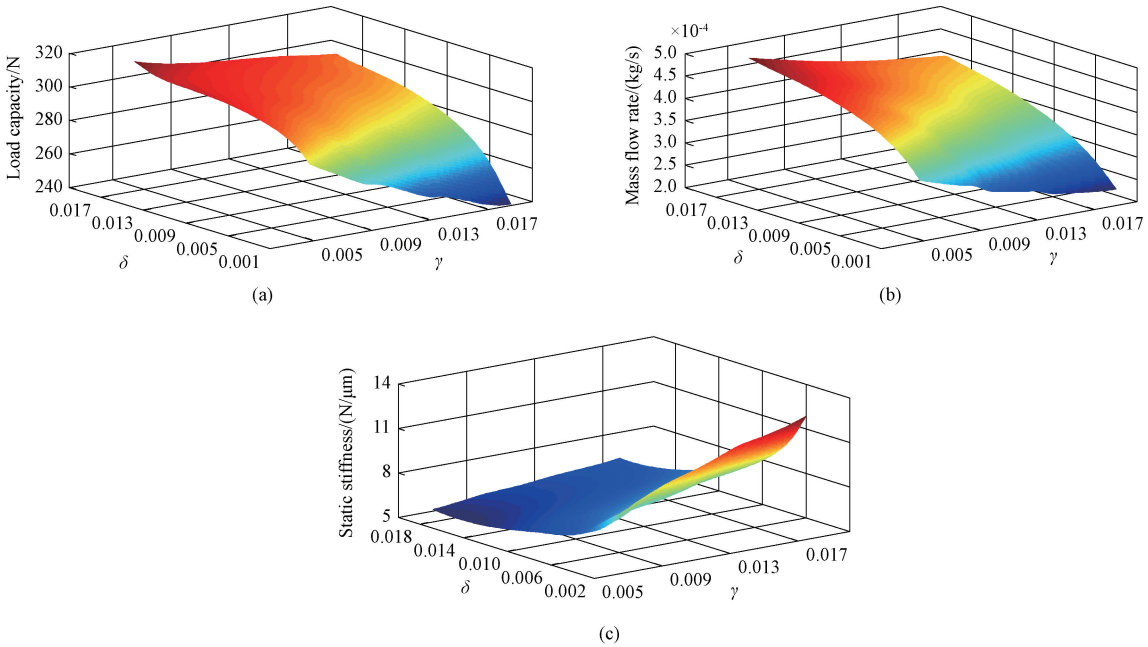

Fig. 3 Relationship among restricted-layer coefficients and static characteristics of bearing: (a) relationship among restricted-layer coefficients and load capacity; (b) relationship between restricted-layer coefficients and mass flow rate; (c) relationship among restricted-layer coefficients and static stiffness

2.3 Performance comparison between restricted-layer and unrestricted-layer aerostatic porous bearings

To achieve both high load capacity and static stiffness in the aerostatic porous bearing, a comparative analysis of bearing performance with varying permeability levels should be conducted, with particular emphasis on the role of the coarse layer. Drawing on the foregoing discussed values of δ and γ, the performance comparison between bearings with a restricted layer and those with different permeabilities in case of different bearing clearances is made. Figure 4 illustrates that the load capacity and static stiffness decrease but the mass flow rate increases with the bearing clearance increasing. The lower the permeability of the coarse-layer porous material, the greater the decline of the load capacity for the unrestricted-layer aerostatic porous bearing. The unrestricted-layer aerostatic porous bearing with a permeability of 10^{-12} m^2 presents a rather low static stiffness and considerably high mass flow rate, though its load capacity is superior to other bearings. Additionally, the unrestricted-layer aerostatic porous bearing with a permeability of 10^{-14} m^2 exhibits a high static stiffness when the bearing clearance is less than 9 μm. Nevertheless, this inevitably requires operation under extremely narrow bearing clearance conditions, which requires considerably high manufacturing accuracy. By comparison, the restricted-layer aerostatic porous bearing not only retains a relatively higher load capacity but also has a lower mass flow rate. In particular, when the bearing clearance is higher than 15 μm, the static stiffness of the restricted-layer aerostatic porous bearing steadily exceeds that of other bearings, while the load capacity and static stiffness of the unrestricted-layer aerostatic porous bearing at a permeability of 10^{-14} m^2 gradually become inferior. Therefore, the bearing with a restricted layer takes on better practicality and superiority in terms of applicable bearing clearance.

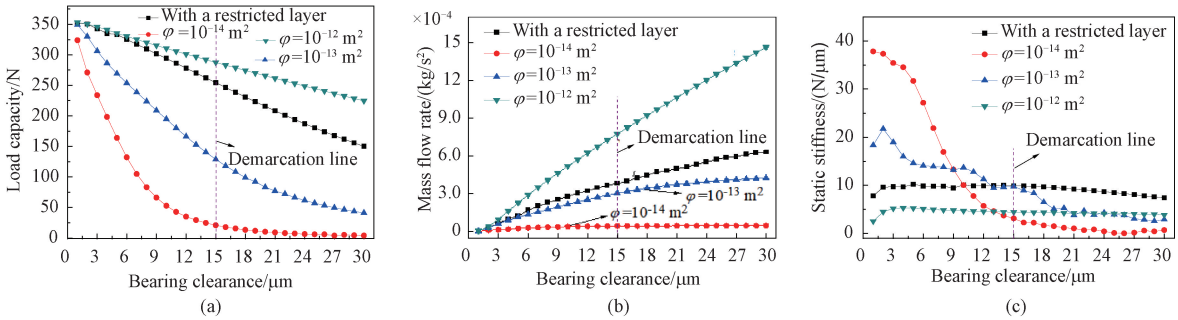

Fig. 4 Static characteristic comparison among bearings with different materials: (a) relationship between bearing clearance and load capacity; (b) relationship between bearing clearance and mass flow rate; (c) relationship between bearing clearance and static stiffness

Figure 5 shows the pressure contour plots on the section through the axe of the coarse layer, which reflects the pressure drop in the porous material. When the compressed gas is fed to the bearing, the pressure drops due to the viscous flow across the porous restrictor. It is obvious that the pressure drop across the unrestricted layer of the porous material gradually aggravates with the permeability decreasing. Furthermore, the higher the bearing clearance is, the sharper the pressure drop in the coarse-layer porous material. In contrast, a large percentage of the pressure drop occurs in the restricted layer of porous material, considerably reducing the viscous loss. Thus, the researchers have the freedom to adjust the geometry of the coarse layer to meet the mechanical requirements.

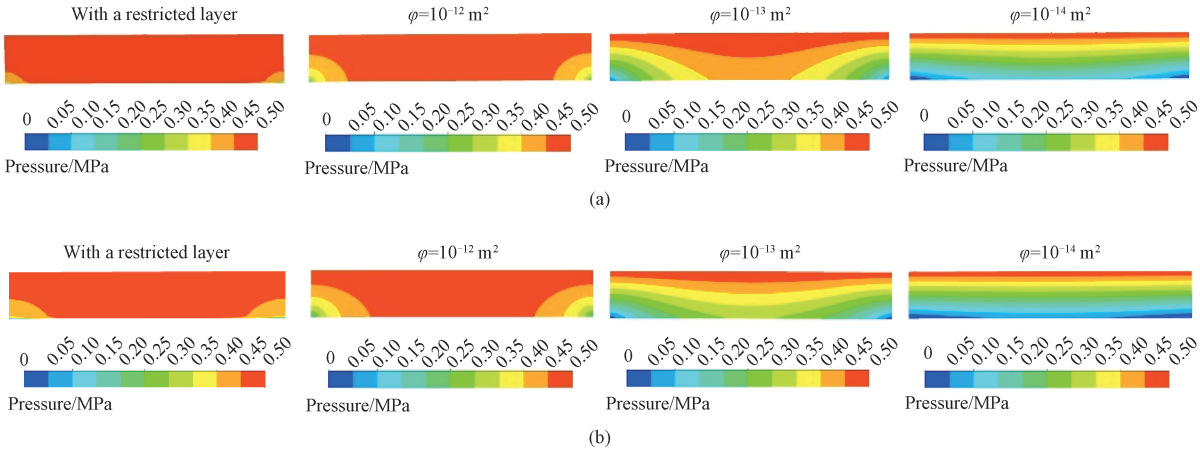

Fig. 5 Comparison of pressure contour plots of different bearings: (a) pressure contour plots at h of 10 μm; (b) pressure contour plots at h of 15 μm

The static characteristics of the bearing are obtained when the bearing clearance is 20 μm and subtracted from that of the bearing with a full gas supply. Figure 6 reveals that the bearing with a low permeability generally shows a relatively low sensitivity to the bearing clearance. Figure 6(c) conveys the abnormal message that when the bearing clearance is less than 12 μm, the mass flow rate difference increases first and then decreases with the increase of the permeability, and the mass flow rate difference of the unrestricted-layer aerostatic porous bearing with a high permeability increases rapidly. In conclusion, the restricted-layer aerostatic porous bearing highlights a small performance difference except for the unrestricted-layer aerostatic porous bearing with a permeability of 10^{-14} m^2 when the gas supply area changes, and especially with the increase of the bearing clearance, the static stiffness difference of all bearings becomes subtle.

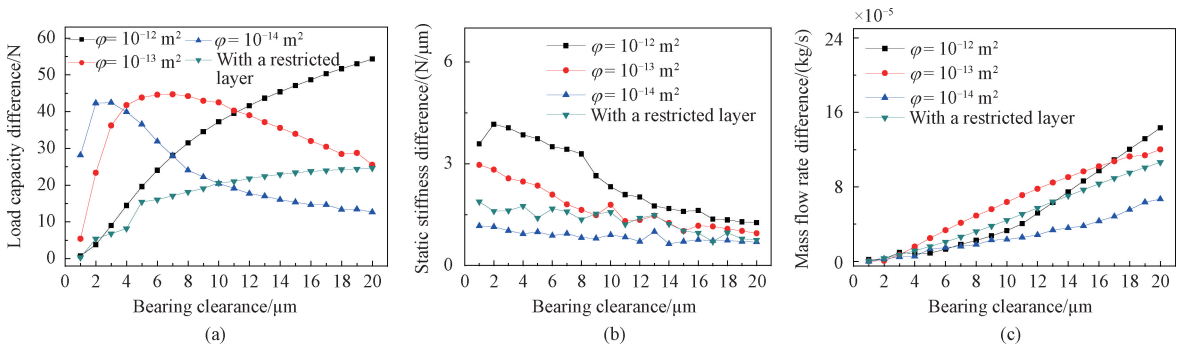

Fig. 6 Bearing performance comparison among bearings with different bearing clearances: (a) relationship between bearing clearance and load capacity difference; (b) relationship between bearing clearance and static stiffness difference; (c) relationship between bearing clearance and mass flow rate difference

3 Conclusions

In this paper, the static characteristics of the restricted-layer aerostatic porous bearing such as the load capacity, static stiffness and mass flow rate are analyzed by theory and Fluent simulation. The conclusions are as follows.

1) Two proportional coefficients, a permeability ratio δ and a thickness ratio γ, are proposed, and a parametric sensitivity analysis shows that when $\delta \approx 0.005$ and $\gamma \approx 0.010$, the load capacity and static stiffness of the restricted-layer aerostatic porous bearing are higher.

2) Compared with the unrestricted-layer aerostatic porous bearing, the existence of the restricted layer not only enhances the throttling effect and reduces the mass flow rate, but also effectively improves the static stiffness of the bearing.

3) The pressure drop mainly occurs on the surface of the restricted layer, which greatly reduces the viscous loss. Thus, the restricted-layer aerostatic porous bearing allows researchers to freely adjust the geometry of the coarse layer to meet the mechanical requirements.

4) The low permeability bearing is less sensitive to changes in the bearing clearance. When the gas supply area changes, the restricted-layer aerostatic porous bearing has a lower difference in performance change than the unrestricted-layer aerostatic porous bearing, and has superior load capacity and static stiffness.

References

[1] CHEN G D, JU B F, FANG H, et al. Air bearing: academic insights and trend analysis [J]. *The International Journal of Advanced Manufacturing Technology*, 2020, 106(3): 1191-1202.

[2] ZHANG K, HU H D, GUO M H, et al. Effects from O-rings on the stability of a rotor-porous air journal bearing test-rig [J]. *Journal of Mechanical Engineering*, 2024, 60: 1-9. (in Chinese)

[3] GU Y D, MARTIN B, ARTUR S, et al. Aerostatic bearing with porous restrictor: research status and future perspectives [J]. *Journal of Drainage and Irrigation Machinery Engineering*, 2021, 39(8): 818-825. (in Chinese)

[4] WANG W, CHENG X H, ZHANG M, et al. Effect of the deformation of porous materials on the performance of aerostatic bearings by fluid-solid interaction method [J]. *Tribology International*, 2020, 150: 106391.

[5] YAN R Z, ZHANG Y B. Static and dynamic characteristics of vacuum preloaded porous aerostatic bearings [J]. *Journal of Donghua University (English Edition)*, 2024, 41(1): 81-88.

[6] SAN ANDRÉS L, YANG J, MCGOWAN R. Measurements of static and dynamic load performance of a 102 MM carbon-graphite porous surface tilting-pad gas journal bearing [J]. *Journal of Engineering for Gas Turbines and Power*, 2021, 143(11): 111017.

[7] KANG L, ZHANG X N, LOU J J, et al. Conjugate heat transfer study on porous media gas lubricated bearing[J]. *Journal of Engineering for Thermal Energy and Power*, 2020, 35(3): 158-166. (in Chinese)

[8] YAMADA K, ONISHI N, SEKIYA K, et al. Permeability control method with laser for porous bushings of aerostatic bearings[J]. *International Journal of Precision Engineering and Manufacturing*, 2013, 14(5): 779-784.

[9] PANZERA T H, CHRISTOFORO A L, CAMPOS RUBIO J C, et al. Evaluation of compacted cementitious composites for porous bearings [J]. *International Journal of Applied Ceramic Technology*, 2013, 10(3): 474-483.

[10] DA SILVA L J, PANZERA T H, VIEIRA L M, et al. Carbon nanotubes and superplasticizer reinforcing cementitious composite for aerostatic porous bearing[J]. *Proceedings of the Institution of Mechanical Engineers, Part J: Journal of Engineering Tribology*, 2017, 231(11): 1397-1407.

[11] MIYATAKE M, YOSHIMOTO S, SATO J. Whirling instability of a rotor supported by aerostatic porous journal bearings with a surface-restricted layer[J]. *Proceedings of the Institution of Mechanical Engineers, Part J: Journal of Engineering Tribology*, 2006, 220(2): 95-103.
[12] CUI C, ONO K. Theoretical and experimental investigation of an externally pressurized porous annular thrust gas bearing and its optimal design [J]. *Journal of Tribology*, 119(3): 486-492.
[13] SAHA N, MAJUMDAR B C. Study of externally-pressurized gas-lubricated two-layered porous journal bearings: a steady state analysis [J]. *Proceedings of the Institution of Mechanical Engineers, Part J: Journal of Engineering Tribology*, 2002, 216(3): 151-158.
[14] YOSHIMOTO S, TOZUKA H, DAMBARA S. Static characteristics of aerostatic porous journal bearings with a surface-restricted layer [J]. *Proceedings of the Institution of Mechanical Engineers, Part J: Journal of Engineering Tribology*, 2003, 217(2): 125-132.
[15] FENG K, LI W J, HUO Y W, et al. Thermal characteristic analysis of aerostatic porous journal bearings with surface-restricted layer[J]. *Journal of Mechanical Engineering*, 2018, 54(12): 216-224. (in Chinese)
[16] OTSU Y, MIYATAKE M, YOSHIMOTO S. Dynamic characteristics of aerostatic porous journal bearings with a surface-restricted layer [J]. *Journal of Tribology*, 2011, 133(1): 011701.
[17] LI Y F, YIN Y H, YANG H, et al. Modeling for optimization of circular flat pad aerostatic bearing with a single central orifice-type restrictor based on CFD simulation [J]. *Tribology International*, 2017, 109: 206-216.

带有限制层多孔质空气轴承静态特性分析

余 哲[1,2], 闫如忠[1,2*], 马晓建[1,2], 张豪杰[1,2]
1. 东华大学 机械工程学院, 上海 201620
2. 东华大学 纺织装备教育部工程研究中心, 上海 201620

摘 要: 为增强气体阻尼效果并提高轴承性能, 可在多孔质空气轴承的表面增加限制层。基于气体润滑理论, 建立了带有限制层多孔质空气轴承的数学模型, 提出了渗透率比 δ 和厚度比 γ 两个比例系数。通过对复杂的限制层参数进行参数敏感性分析得到 δ 和 γ 的临界系数。利用 Fluent 仿真对带有限制层多孔质空气轴承和非限制层多孔质空气轴承的静态特性进行了对比分析。结果表明: 当 $\delta \approx 0.005$、$\gamma \approx 0.010$ 时, 带有限制层多孔质空气轴承的承载能力和静刚度较大; 与非限制层多孔质空气轴承相比, 带有限制层多孔质空气轴承对供气区域变化的敏感度较低。限制层的存在不仅能增强节流效果, 降低空气质量流率, 还能有效提高轴承静刚度。

关键词: 多孔质空气轴承; 限制层; 静态性能; 临界系数